n-type electrical conduction in SnS thin films

Issei Suzuki [1,*], Sakiko Kawanishi [1,†], Sage R. Bauers [2], Andriy Zakutayev [2], Zexin Lin [1], Satoshi Tsukuda [1], Hiroyuki Shibata [1], Minseok Kim [3], Hiroshi Yanagi [3], and Takahisa Omata [1]

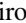[1]*Institute of Multidisciplinary Research for Advanced Materials, Tohoku University, 2-1-1 Katahira, Aoba-ku, Sendai, Miyagi 980-8577, Japan*

[2]*Material Science Center, National Renewable Energy Laboratory, Golden, Colorado 80401, USA*

[3]*Graduate Faculty of Interdisciplinary Research, University of Yamanashi, 4-4-37 Takeda, Kofu, Yamanashi 400-8510, Japan*

Tin monosulfide (SnS) usually exhibits *p*-type conduction due to the low formation enthalpy of acceptor-type defects, and as a result, *n*-type SnS thin films have never been obtained. In this paper, we realize *n*-type conduction in SnS thin films by using radiofrequency-magnetron sputtering with Cl doping and a sulfur plasma source during deposition. Here, *n*-type SnS thin films are obtained at all the substrate temperatures employed in this paper (221–341 °C), exhibiting carrier concentrations and Hall mobilities of $\sim 2 \times 10^{18}$ cm^{-3} and 0.1–1 cm^2 V^{-1} s^{-1}, respectively. The films prepared without a sulfur plasma source, on the other hand, exhibit *p*-type conduction despite containing a comparable amount of Cl donors. This is likely due to a significant number of acceptor-type defects originating from sulfur deficiency in *p*-type films, which appears as a broad optical absorption within the band gap. We demonstrate *n*-type SnS thin films in this paper for the realization of SnS homojunction solar cells, which are expected to have a higher conversion efficiency than the conventional heterojunction SnS solar cells.

I. INTRODUCTION

Controlling the electrical properties of semiconductors by impurity doping is one of the most important techniques in semiconductor technologies. This technique could allow carrier-type conversion between the *p*- and *n*-type carriers and thus the formation of a *pn* homojunction. In nominally undoped semiconductors, the carrier type is generally determined by the defects with a low formation enthalpy and low ionization energy, and this often makes carrier-type conversion difficult. The history of GaN-based blue light-emitting diodes (LEDs) is a good example. Carrier-type conversion of intrinsically *n*-type GaN to *p*-type by impurity doping had been the primary obstacle, and therefore, its achievement was the biggest breakthrough for the realization of blue LEDs [1], leading to a Noble Prize in physics in 2014.

Tin monosulfide (SnS) is a promising material for the solar light absorber for thin film solar cells because it is composed of abundant and nontoxic elements and exhibits an appropriate optical property for solar cells. SnS usually exhibits *p*-type conduction due to the intrinsic defects. Under S-rich conditions, the acceptor-type Sn vacancy (V$_{Sn}$) is easily formed.

Under S-poor conditions, Sn tends to migrate into the vacant S sites, and then acceptor-type V$_{Sn}$ and Sn antisites (Sn$_S$) are easily formed. Regardless of the conditions, S vacancy (V$_S$) is an ambipolar defect with deep states that can trap both electrons and holes [2–4]. Therefore, there has been a long challenge to realize the *n*-type SnS thin film by impurity doping. However, substitutional cation doping of Sn^{2+} with trivalent cations, such as Sb^{3+} and Bi^{3+}, did not lead to *n*-type conduction [4–6]. The fabrication of *n*-type SnS thin films thus remained elusive to date.

Recently, in SnS bulk pellets and single crystals, it was found that substitutional anion doping of S^{2-} with halide ions, such as Cl$^-$ and Br$^-$, successfully achieved *n*-type electrical conduction [7–11]. This doping approach is more suitable for practical use than the solid solutions between SnS and PbS (Sn$_{1-x}$Pb$_x$S), which are the only SnS-containing *n*-type semiconductors reported before the halogen-doped SnS [12,13] and unfortunately contains a large amount of toxic Pb ($x > 0.2$).

Compared with bulk *n*-type SnS, the difficulty in fabricating *n*-type SnS thin films by physical vapor deposition (such as sputtering, pulsed laser deposition, or thermal evaporation) is likely related to the preferential formation of intrinsic defects under the deposition atmosphere. Because the vapor pressure of elemental sulfur is 11 orders of magnitude higher than that of elemental tin at 500 °C [14], SnS thin films prepared in the open system of physical vapor deposition are probably more prone to sulfur deficiency than the bulk SnS prepared in a substantially closed system. Accordingly, it is hypothesized that acceptor-type defects (V$_{Sn}$ and Sn$_S$) and ambipolar defects (V$_S$), both caused by sulfur deficiencies,

---

*Corresponding author: issei.suzuki@tohoku.ac.jp

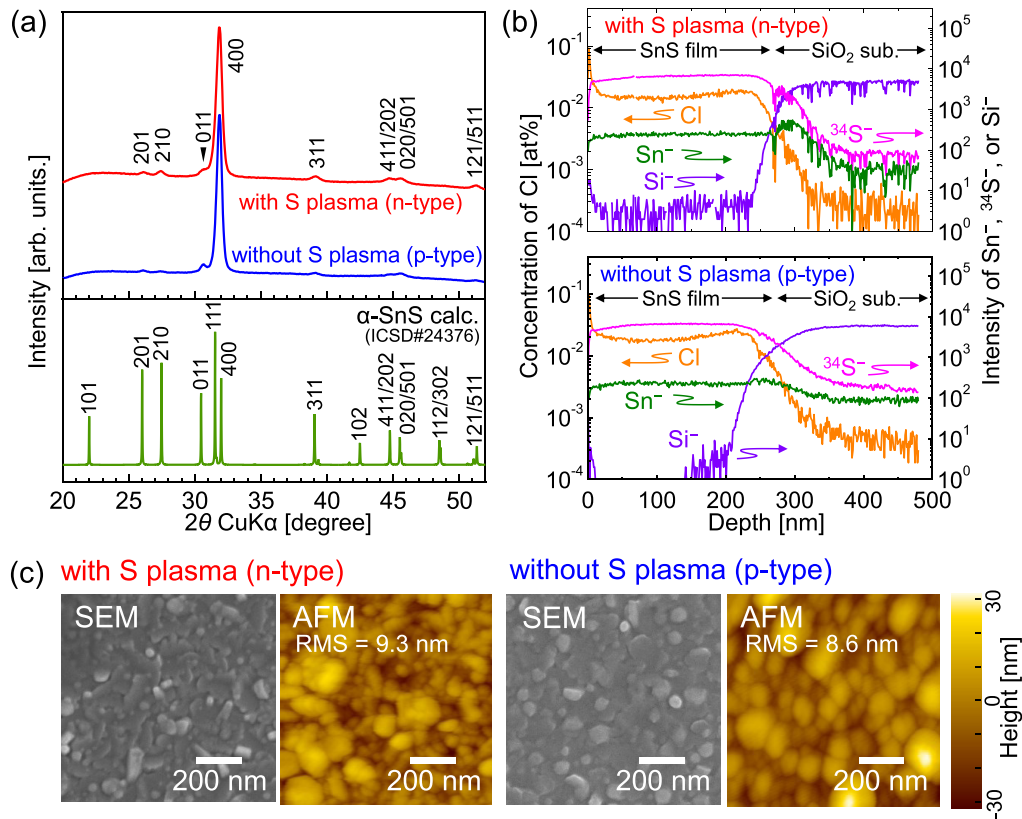†Corresponding author: s-kawa@tohoku.ac.jp

FIG. 1. Structural, compositional, and morphological analysis of Cl-doped SnS thin films deposited with and without a sulfur plasma supply. (a) X-ray diffraction (XRD) profiles of films deposited at $T_{sub} = 333\,°C$, together with a reference pattern of α-SnS (ICSD#24376). (b) Depth profile of Cl concentration and normalized intensities of secondary ions of Sn^-, $^{34}S^-$, and Si^- in the films deposited at $T_{sub} = 333\,°C$. (c) Scanning electron microscopy (SEM) and atomic force microscopy (AFM) images of the surface of SnS thin films deposited at $T_{sub} = 333\,°C$. The root-mean-square (RMS) roughness is also shown. Additional SEM and AFM images are available in Fig. S6 in the Supplemental Material [16].

compensate the electrons introduced by halogen doping, preventing the halogen-doped SnS thin films from exhibiting *n*-type conduction. Innovative thin film deposition methods are needed to address this challenge.

Herein, *n*-type SnS thin films were fabricated by radiofrequency (RF) magnetron sputtering together with an RF sulfur plasma source. The additional sulfur plasma supplied to the films during deposition increased the sulfur content of the resulting films. It was found that using the sulfur plasma source during deposition significantly suppressed the formation of acceptor-type defects in the SnS films, presumably V_{Sn} and Sn_S, as well as ambipolar V_S. This is the key to realize *n*-type conduction in Cl-doped SnS thin films. The fabrication technique demonstrated here for *n*-type SnS thin films is expected to revolutionize SnS solar cells, from heterojunctions developed over the last two decades to homojunctions with much higher efficiency.

II. EXPERIMENTAL

SnS thin films were fabricated by RF-magnetron sputtering. To investigate the substrate temperature dependence of the physical properties of SnS thin films, a SiO_2 glass substrate (50 × 50 mm) with a temperature gradient across it (221–341 °C) [15] was used (for the spatial distribution of

substrate temperature, see Fig. S1 in the Supplemental Material [16]). The deposition time was 30 min. A 2-inch-diameter piece of undoped SnS (99.99%, Advanced Engineering Materials) was used as the sputtering target. Before thin film deposition, Cl was supplied to the deposition vacuum chamber by exposing a Cl-containing SnS target [Cl/(SnS + Cl) = 0.1, 99.99%, Advanced Engineering Materials] to Ar plasma for 30 min under the same conditions as the thin film deposition, during which a temporary substrate was set on the substrate holder. Then the deposition chamber was evacuated to its base pressure ($<5 \times 10^{-4}$ Pa), and the substrate was replaced. A sulfur plasma source (RF solid plasma source RFK30, Oxford Applied Research) was used in conjunction with RF sputtering to avoid sulfur deficiency in the resulting thin films. Further details of the thin film fabrication (such as the specific sputtering conditions, configuration of the deposition equipment, and operating conditions of the sulfur plasma source) are available in Sec. S2 in the Supplemental Material [16] together with details of the thin film characterization methods.

III. RESULTS AND DISCUSSION

The thin film prepared at a substrate temperature (T_{sub}) of 333 °C is firstly discussed as a representative sample. As shown in Fig. 1(a), all x-ray diffraction (XRD) peaks of

TABLE I. Physical properties of SnS thin films prepared at $T_{sub} = 333\,°C$ with and without a sulfur plasma supply. All results were obtained at room temperature, except that the Seebeck coefficients were measured at 25–50 °C.

	SnS thin films deposited	
	With sulfur plasma	Without sulfur plasma
Thickness (nm)	250	190
Atomic ratio, S/(Sn + S)	0.507	0.498
Cl concentration (cm^{-3})	3.7×10^{18}	4.6×10^{18}
Hall coefficient (cm^3 C^{-1})	-2.6×10^{0}	$+4.8 \times 10^{3}$
Seebeck coefficient (μV K^{-1})	-6.3×10^{1}	$+1.4 \times 10^{4}$
Carrier type	*n*-type	*p*-type
Electrical conductivity (S cm^{-1})	9.2×10^{-2}	3.1×10^{-4}
Carrier concentration (cm^{-3})	2.4×10^{18}	1.4×10^{15}
Hall mobility (cm^2 V^{-1} s^{-1})	2.4×10^{-1}	1.5×10^{0}

the obtained films are indexed as α-SnS (see Fig. S3 in the Supplemental Material [16] for the crystal structure), and no impurity phases such as polymorphs of SnS, SnS$_2$, and Sn$_2$S$_3$ were observed whether sulfur plasma was supplied or not during deposition. The intense peak observed at around $2\theta = 32\,°$ corresponds to the 400 diffraction peak of α-SnS. This peak has a much stronger intensity than the others, indicating that the obtained SnS films exhibited preferential (100) orientation at $T_{sub} = 333\,°C$. This result is consistent with the orientation mappings obtained by electron backscattered diffraction (EBSD, see Fig. S4 in the Supplemental Material [16]).

The chemical compositions of the films deposited with and without sulfur plasma supply were evaluated by x-ray fluorescence spectroscopy (XRF) [17]. Their compositions were close to the stoichiometry of SnS [S/(Sn + S) = 0.5], as indicated in Table I. Figure 1(b) shows the depth profile of Cl concentration and the intensities of secondary ions of Sn$^-$, ^{34}S$^-$, and Si$^-$ determined by time-of-flight secondary ion mass spectroscopy (TOF-SIMS). The concentrations of Sn, S, and Cl were almost uniform in the thickness direction, regardless of sulfur plasma supply. The Cl concentrations shown in Table I were obtained by averaging the bulk part of the *n*- and *p*-type SnS thin films [70–110 nm from the surface in Fig. 1(b)]. The in-plane analysis by TOF-SIMS also showed uniform distribution of each element over a film area of $100 \times 100\,\mu$m, thereby excluding the possibility of segregation due to impurity phases (see Fig. S5 in the Supplemental Material [16]). All results of phase identification and chemical compositional analysis support that the obtained films consist of a uniform single-phase α-SnS.

In Fig. 1(c), both surface scanning electron microscopy (SEM) and atomic force microscopy (AFM) observations indicate that the obtained SnS films are composed of almost circular grains with a diameter of 10 to 200 nm regardless of sulfur plasma supply, while grain size tends to be slightly smaller in the film deposited with sulfur plasma supply ($<$100 nm). The obtained SnS thin films consisted of much finer grains as SnS thin films prepared by RF-magnetron sputtering than the previous reports [18,19].

The electrical properties are also summarized in Table I. The SnS thin film prepared with sulfur plasma supply showed negative values of both Hall and Seebeck coefficients, which

indicate *n*-type conduction. On the other hand, the film prepared without sulfur plasma supply had positive values for both coefficients, indicating *p*-type conduction. Furthermore, the Fermi level shift in the electronic structure was directly observed by bulk-sensitive x-ray photoelectron spectroscopy (XPS) measured with monochromatic Ag Lα excitation ($h\nu = \sim$3 keV). As shown in Fig. 2(a), the binding energies of the valence band edge, S $2p$, and Sn $3d$ peaks of the film deposited with sulfur plasma supply (the *n*-type film) shifted downward by $\sim$0.3 eV compared with that without sulfur plasma (*p*-type), which is direct evidence that the Fermi level of the *n*-type film is 0.3 eV closer to the conduction band edge than the *p*-type film. These results show that the presence or absence of sulfur plasma supply determines the carrier type of the thin films.

It is interesting to note that *n*-type conduction in SnS thin films could be achieved by supplying sulfur plasma during deposition together with Cl doping but not by Cl doping alone. The carrier concentration of the *n*-type film is close to the Cl donor concentration (Table I), suggesting that carrier electrons are generated by Cl doping, and the activation efficiency of the Cl donors in this film is as high as $\sim$65%. The film prepared without sulfur plasma had a similar Cl concentration; however, it did not exhibit *n*-type conduction. This clearly indicates that *n*-type conduction in SnS thin films cannot be achieved only by incorporating Cl donors, likely due to compensation by intrinsic defects.

Other important features and clues related to Cl incorporation and defect compensation were observed in the optical absorption spectra of these films. In Fig. 2(b), in addition to the steep slope starting from 1.3 eV corresponding to the fundamental absorption of SnS, a broad absorption centered at $\sim$1.1 eV was much more obvious in the film deposited without supplying sulfur plasma (*p*-type film) than the film deposited with it (*n*-type film). This broad absorption is distinguished from interband transitions in the $h\nu$ vs $(\alpha h\nu)^{1/r}$ plots, where $h\nu$, α, and r are the photon energy, absorption coefficient, and an index related to the interband transition type, respectively [20] (see Fig. S8 in the Supplemental Material [16]). This indicates the presence of many in-gap states in the *p*-type films deposited without sulfur plasma supply. Since this absorption was not obvious in the *n*-type film prepared with sulfur plasma
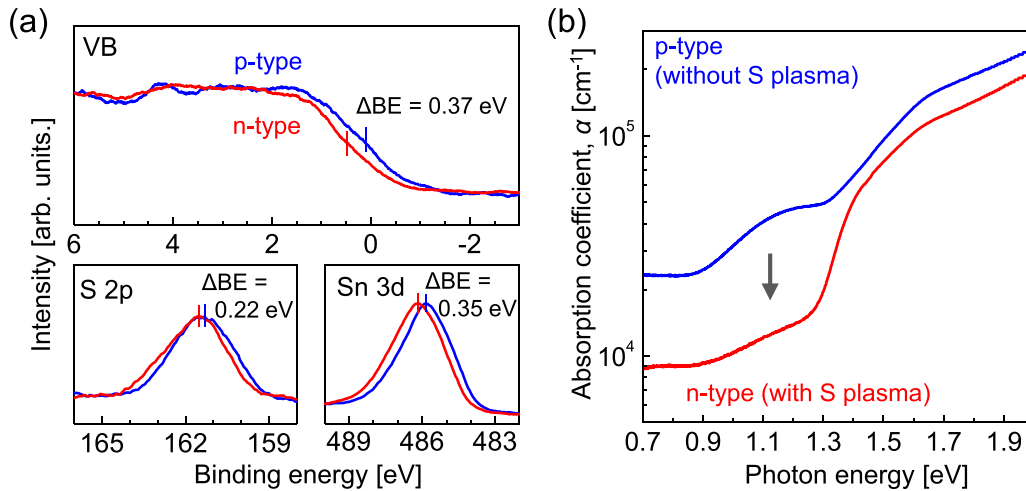
FIG. 2. (a) X-ray photoelectron spectroscopy (XPS) spectra (excitation source: Ag Lα) of SnS films deposited at $T_{sub} = 222\,^{\circ}$C for the valence band (VB), S $2p$, and Sn $3d$ core levels. Differences in the binding energies between *n*- and *p*-type films (ΔBE) are shown in each plot. A total resolution of $\sim$0.5 eV for the measurement resulted in significant spectral broadening. The displayed spectra were obtained by the moving average of the original results, which are available in Fig. S7 in the Supplemental Material [16]. Other characteristics of this film ($T_{sub} = 222\,^{\circ}$C) are discussed in the last half of main text. (b) Absorption spectra of the *n*- and *p*-type SnS thin films prepared at $T_{sub} = 333\,^{\circ}$C. The broad peak centered at 1.1 eV is significant only for the *p*-type film.

supply, it should be related to the defects associated with the sulfur deficiency.

According to first-principles calculations [2–4], Sn$_S$ and V$_{Sn}$ are the most likely defects formed under sulfur-deficient conditions, and they act as acceptors. In addition, V$_S$ is an ambipolar defect that can also compensate donors when the Fermi level is high in the gap. Therefore, the broad and strong absorption in the *p*-type film ought to be related to the in-gap states due to Sn$_S$, V$_{Sn}$, V$_S$, or their complex with Cl impurities (such as Sn$_S$-Cl$_S$, V$_{Sn}$-Cl$_S$, or V$_S$-Cl$_S$). The SnS thin film will not exhibit *n*-type conduction even with halogen doping if such defects are present at a high concentration. Sulfur deficiency is commonly observed in SnS thin films prepared by physical vapor deposition [21–23]. Postanneal of the sulfur-deficient SnS thin films in an atmosphere with high sulfur activity, such as H$_2$S, cannot effectively reduce the concentration of holes (i.e., acceptor-type defects) [24]. Therefore, it is supposed that supplying highly reactive sulfur (i.e., sulfur plasma) during film deposition, which was employed in this paper, is essential for realizing *n*-type conduction in Cl-doped SnS thin films.

Figure 3(a) plots the temperature-dependent carrier concentration in the *n*- and *p*-type films. Carrier concentration of the *p*-type film showed thermally activated behavior with an activation energy of $E_a = 230$ meV, which is comparable with those of undoped *p*-type SnS thin films from previous reports ($E_a = \sim$300 meV [25,26]). The *n*-type film exhibited almost no temperature dependence, indicating that the film is an almost degenerated semiconductor. Like the control of carrier concentration in *n*-type SnS bulk ceramics by the Cl doping level, [11] the carrier concentration of *n*-type films should also be controllable by the amount of incorporated Cl donor. Figure 3(b) shows temperature dependence of the Hall mobility for the films. The Hall mobility decreases with decreasing temperature for both *n*- and *p*-type SnS thin films. The $\log(\mu_{Hall}T^{1/2}) - T^{-1}$ plot exhibits a straight line, suggesting that grain boundary scattering dominates carrier transport in the films [27]. This is consistent with the fact that carrier transport is not dominated by ionized scattering or phonon scattering in these films (see Fig. S9 in the Supplemental Material [16] for double-log plots of Hall mobility and temperature). The calculated potential barriers at the grain boundary (Φ_B) are 70 and 55 meV for *n*- and *p*-type SnS thin films, respectively, which are of the same order of magnitude as values previously reported for undoped *p*-type SnS thin films that are dominated by grain boundary scattering ($\Phi_B = 50$–70 meV [28,29]). The main reason for the dominance of grain boundary scattering in the obtained films is their small grain sizes [which were discussed above, see Fig. 1(c)], which lead to many grain boundaries. It has been reported in several SnS studies that the carrier mobility of SnS thin films increases with increasing grain size [18,30,31], which is also a general property of polycrystalline thin films with dominant grain boundary scattering [32]. The morphology of the SnS thin films strongly depends on the deposition conditions, especially the sputtering pressure. The films deposited at relatively low pressures $\leqslant \sim$1 Pa, as the pressure used in this paper (0.35 Pa), tend to be flatter with finer grains, while those deposited at high pressures ($\geqslant \sim$1 Pa) possess larger grains and rougher surfaces [18,19]. Therefore, optimizing the sputtering conditions would allow the deposition of films with larger grains and correspondingly higher carrier mobility.

Substrate temperature dependence (221–341 $^{\circ}$C) of physical properties of SnS thin films was also investigated. The films prepared with and without sulfur supply exhibited *n*- and *p*-type conduction, respectively, regardless of the substrate temperature (for the electrical properties of each sample, see Fig. S10 and Tables S4 and S5 in the Supplemental Material [16]). The obtained films were of single-phase α-SnS and exhibited preferential (100) orientations regardless of the
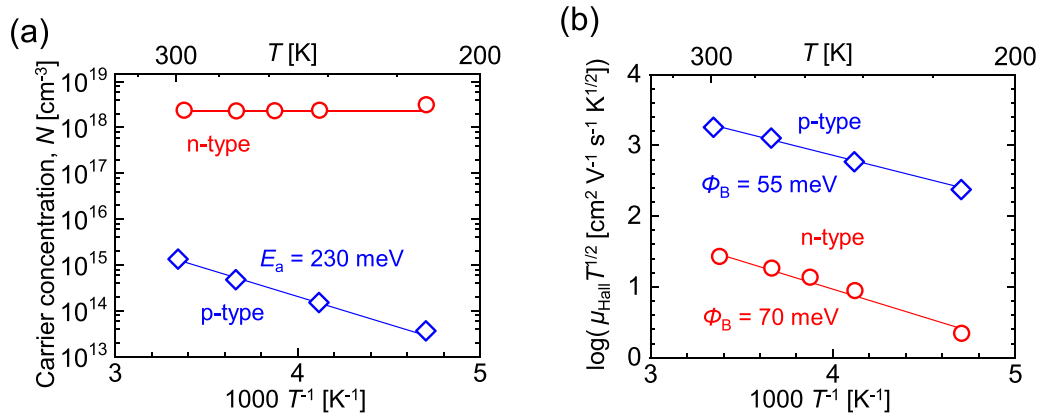
FIG. 3. (a) Temperature dependence of carrier concentration and (b) $\mu_{Hall}T^{1/2}$ of SnS thin films deposited at $T_{sub} = 333\,°C$. The activation energy (E_a) and grain boundary potential barriers (Φ_B) were estimated according to the following formulas: $N = N_0 \exp(-E_a/kT)$, where N_0 is a prefactor and k is the Boltzmann constant, and $\mu_{Hall} = Le(1/2\pi m^* kT)^{1/2} \exp(-\Phi_B/kT)$, where L is the grain size, e is elementary charge, and m^* is the effective mass. The solid lines were added to guide the eye.

substrate temperature (see Figs. S11 and S12 in the Supplemental Material [16] for XRD profiles of out-of-plane (2θ) and in-plane ($2\theta_\chi$), respectively). The primary peaks corresponding to 400 diffractions shifted toward lower diffraction angle with decreasing the substrate temperature, indicating that the lattice constant in the a axis, a_0, increased with decreasing the substrate temperature, as shown in Fig. 4(a). The thicknesses of the obtained films were 250–260 and 190–200 nm when deposited with and without sulfur plasma, respectively (see details in Fig. S13 in the Supplemental Material [16]), and therefore, supplying sulfur plasma increases the deposition rate by ~30%.

Figure 4(b) plots the chemical composition of SnS thin films against the substrate temperature. The composition is almost independent of the substrate temperature, and supplying sulfur plasma slightly increased sulfur content in the resulting films by ~1%. The broad optical absorption related to the defect levels associated with acceptor-type defects [which were discussed above, see Fig. 2(b)] was observed in all *p*-type SnS films at similar intensities, whereas they were hardly visible in the *n*-type films at any substrate temperature (see Fig. S8 in the Supplemental Material [16]). Therefore, changing the substrate temperature cannot suppress the formation of acceptor-type defects due to sulfur deficiency, while supplying sulfur plasma is always effective in suppressing these defects and leads to *n*-type conduction at any substrate temperature employed in this paper.

Figures 4(c) and 4(d) show the substrate temperature dependence of the electrical properties for both *n*- and *p*-type SnS thin films. The carrier concentrations of *n*-type films did not depend on the substrate temperature (~$2 \times 10^{18}\,cm^{-3}$), implying that all these films had comparable Cl concentration. The Hall mobility of the *p*-type thin films did not depend on the temperature either, whereas the *n*-type films exhibited a convex trend with a maximum at $T_{sub} \sim 260\,°C$. Their carrier type, chemical composition, and number of acceptor-type defects were not affected significantly by the substrate temperature but rather by whether sulfur plasma was supplied during the deposition. These results indicate that the fabrication process of *n*-type SnS thin films demonstrated here could be applied under a wide range of sputtering

conditions. The *n*-type SnS thin films obtained in this paper have a high carrier concentration and low Hall mobility compared with the previously reported *p*-type films and *n*-type bulk single crystals, as shown in Fig. 4(e). By tuning the deposition conditions, the proposed fabrication process using sulfur plasma supply has high potential for realizing *n*-type SnS thin films with characteristics that are favorable for device applications, for instance, lower carrier concentration and longer minority carrier diffusion length.

Thin film SnS is expected to be a solar light absorber for next-generation solar cells because of its abundant and nontoxic constitutional elements and suitable optical properties for photovoltaic applications. Due to a lack of *n*-type SnS thin films, SnS thin film solar cells based on the heterojunction structure between *p*-type SnS and other *n*-type semiconductors, such as CdS [33–35] or Zn(O,S) [24,36,37], have been intensively studied in the last two decades. However, due to their unfavorable conduction band offset [35,38] and possible Fermi level pinning induced by defects at the heterojunction interface [34], SnS heterojunction solar cells have a relatively low open-circuit voltage ($V_{OC} = 300–400\,mV$) compared with its band gap energy (~1.1 eV), leading to low conversion efficiencies (η) of only 4–5% at the most [39]. The *pn* homojunction of SnS employing *n*-type SnS thin film developed in this paper is ideally free from these problems, making it the most promising way to improve the open-circuit voltage and conversion efficiency [13,40]. This expectation is supported by the recent study of a prototype SnS homojunction solar cell with halogen-doped *n*-type SnS single crystal and *p*-type SnS thin film exhibited V_{OC} comparable with the highest values for heterojunctions, without optimizing the device structure or fabrication process [41].

In addition, supplying sulfur plasma during deposition is beneficial for the fabrication of high-quality undoped *p*-type SnS thin films because it can effectively suppress the formation of acceptor-type defects. Therefore, undoped *p*-type SnS thin films fabricated under a Cl-free atmosphere would have a lower concentration of defects that act as effective recombination centers and be suitable for solar cell applications. In other words, a sulfur plasma supply can be employed to produce high-quality thin films with both *n*- and *p*-type conduction.
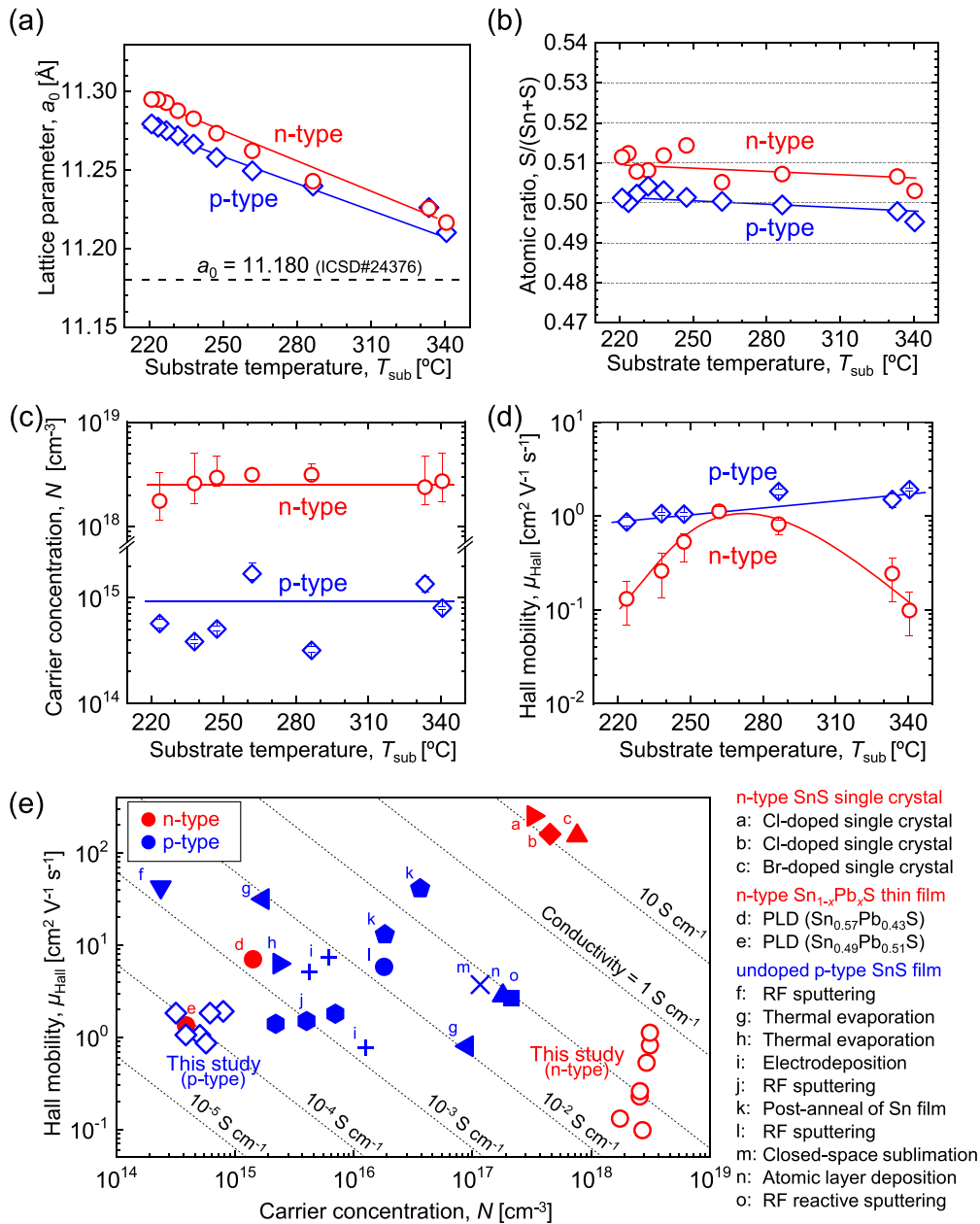
FIG. 4. Substrate temperature dependence of the various properties of the obtained SnS thin films. (a) Lattice parameter of a_0 of the obtained thin films determined by 400 diffraction peaks (for the x-ray diffraction (XRD) profiles, see Fig. S11 in the Supplemental Material [16]). (b) Chemical composition determined by x-ray fluorescence spectroscopy (XRF). (c) Carrier concentration and (d) Hall mobility of SnS thin films measured at room temperature. All solid lines in the figures were added to guide the eye. Detailed data on the electrical properties are available in Fig. S10 and Tables S4 and S5 in the Supplemental Material [16]. (e) Comparison of electrical properties of *n*- and *p*-type SnS thin films obtained in this paper and those of previously reported *n*- and *p*-type SnS, and *n*-type $Sn_{1-x}Pb_xS$ solid solutions. The literature results came from [a]Ref. [8], [b,c]Ref. [9], [d,e]Ref. [13], [f]Ref. [19], [g]Ref. [42], [h]Ref. [43], [i]Ref. [44], [j]Ref. [18], [k]Ref. [45], [l]Ref. [41], [m]Ref. [21], [n]Ref. [46], and [o]Ref. [47].

Consequently, this method will surely be key for realizing highly efficient SnS homojunction solar cells.

IV. CONCLUSIONS

In this paper, we realized *n*-type electrical conduction in SnS thin films by supplying sulfur plasma during the deposition together with Cl doping. Without sulfur plasma supply, the prepared SnS thin films exhibited *p*-type conduction despite containing a comparable amount of Cl donors, and the broad optical absorption of those films would be attributed to the acceptor-type defects originating from sulfur deficiency. Accordingly, both Cl doping and the supply of highly reactive sulfur plasma during deposition are essential to realize *n*-type conduction in SnS thin films. The reported fabrication method can be applied to a wide range of sputtering condi-

tions since *n*-type conduction was obtained regardless of the substrate temperature. So far, the conversion efficiency of SnS heterojunction solar cells is stagnant at low values (4–5%). Methods to fabricate *n*-type SnS thin films will enable SnS *pn* homojunctions and contribute to a change in the SnS solar cell technology from heterojunctions to homojunctions to realize high conversion efficiency.

[1] H. Amano, M. Kito, K. Hiramatsu, and I. Akasaki, *p*-type conduction in Mg-doped GaN treated with low-energy electron beam irradiation (LEEBI), Jpn. J. Appl. Phys. **28**, L2112 (1989).

[2] J. Vidal, S. Lany, M. D'Avezac, A. Zunger, A. Zakutayev, J. Francis, and J. Tate, Band-structure, optical properties, and defect physics of the photovoltaic semiconductor SnS, Appl. Phys. Lett. **100**, 032104 (2012).

[3] Z. Xiao, F.-Y. Ran, M. Liao, H. Hiramatsu, K. Ide, H. Hosono, and T. Kamiya, Multiple states and roles of hydrogen in *p*-type SnS semiconductors, Phys. Chem. Chem. Phys. **20**, 20952 (2018).

[4] B. D. Malone, A. Gali, and E. Kaxiras, First principles study of point defects in SnS, Phys. Chem. Chem. Phys. **16**, 26176 (2014).

[5] P. Sinsermsuksakul, R. Chakraborty, S. B. Kim, S. M. Heald, T. Buonassisi, and R. G. Gordon, Antimony-doped tin(II) sulfide thin films, Chem. Mater. **24**, 4556 (2012).

[6] A. Dussan, F. Mesa, and G. Gordillo, Effect of substitution of Sn for Bi on structural and electrical transport properties of SnS thin films, J. Mater. Sci. **45**, 2403 (2010).

[7] H. Yanagi, Y. Iguchi, T. Sugiyama, T. Kamiya, and H. Hosono, *n*-type conduction in SnS by anion substitution with Cl, Appl. Phys. Express **9**, 051201 (2016).

[8] Y. Iguchi, K. Inoue, T. Sugiyama, and H. Yanagi, Single-crystal growth of Cl-doped *n*-type SnS using SnCl₂ self-flux, Inorg. Chem. **57**, 6769 (2018).

[9] S. Kawanishi, I. Suzuki, T. Ohsawa, N. Ohashi, H. Shibata, and T. Omata, Growth of large single crystals of *n*-type SnS from halogen-added Sn flux, Cryst. Growth Des. **20**, 5931 (2020).

[10] X. Hu, W. He, D. Wang, B. Yuan, Z. Huang, and L.-D. Zhao, Thermoelectric transport properties of *n*-type tin sulfide, Scr. Mater. **170**, 99 (2019).

[11] Y. Iguchi, T. Sugiyama, K. Inoue, and H. Yanagi, Segregation of chlorine in *n*-type tin monosulfide ceramics: actual chlorine concentration for carrier-type conversion, Appl. Phys. Lett. **112**, 202102 (2018).

[12] Z. Xiao, F.-Y. Ran, H. Hosono, and T. Kamiya, Route to *n*-type doping in SnS, Appl. Phys. Lett. **106**, 152103 (2015).

[13] F.-Y. Ran, Z. Xiao, Y. Toda, H. Hiramatsu, H. Hosono, and T. Kamiya, *n*-type conversion of SnS by isovalent ion substitution: geometrical doping as a new doping route, Sci. Rep. **5**, 10428 (2015).

[14] R. E. Honig and D. A. Kramer, Vapor pressure data for the solid and liquid elements, RCA Rev. **30**, 285 (1969).

[15] A. Subramaniyan, J. D. Perkins, R. P. O'Hayre, S. Lany, V. Stevanovic, D. S. Ginley, and A. Zakutayev, Non-equilibrium deposition of phase pure Cu₂O thin films at reduced growth temperature, APL Materials **2**, 022105 (2014).

[16] See Supplemental Material at http://link.aps.org/supplemental/10.1103/PhysRevMaterials.5.125405 for detailed information on thin film fabrication and characterization, temperature gradient in the substrate, crystal structure, EBSD mapping, in-plane analysis by TOF-SIMS measurement, additional SEM and AFM images of thin film morphology, XPS with Ag-Lα excitation, optical properties and determination of band gaps, double log plots of Hall mobility vs temperature, detailed dependence of electrical properties on substrate temperature, and XRD profiles of SnS thin films deposited at various substrate temperatures and thickness of thin films, which includes Ref. [48].

[17] L. L. Baranowski, P. Zawadzki, S. Christensen, D. Nordlund, S. Lany, A. C. Tamboli, L. Gedvilas, D. S. Ginley, W. Tumas, E. S. Toberer, and A. Zakutayev, Control of doping in Cu₂SnS₃ through defects and alloying, Chem. Mater. **26**, 4951 (2014).

[18] V. K. Arepalli, Y. Shin, and J. Kim, Influence of working pressure on the structural, optical, and electrical properties of RF-sputtered SnS thin films, Superlattices Microstruct. **122**, 253 (2018).

[19] B. H. Baby and D. Bharathi Mohan, The effect of *in-situ* and post deposition annealing towards the structural optimization studies of RF sputtered SnS and Sn₂S₃ thin films for solar cell application, Sol. Energy **189**, 207 (2019).

[20] J. Tauc, R. Grigorovici, and A. Vancu, Optical properties and electronic structure of amorphous germanium, Phys. Status Solidi B **15**, 627 (1966).

[21] F. Guastavino Yanuar, C. Llinares, K. Djessas, and G. Masse, SnS thin films grown by close-spaced vapor transport, J. Mater. Sci. Lett. **19**, 2135 (2000).

[22] F.-Y. Ran, Z. Xiao, H. Hiramatsu, K. Ide, H. Hosono, and T. Kamiya, SnS thin films prepared by H_2S-free process and its *p*-type thin film transistor, AIP Adv. **6**, 015112 (2016).

[23] M. Devika, N. K. Reddy, K. Ramesh, K. R. Gunasekhar, E. S. R. Gopal, and K. T. R. Reddy, Influence of annealing on physical properties of evaporated SnS films, Semicond. Sci. Technol. **21**, 1125 (2006).

[24] H. H. Park, R. Heasley, L. Sun, V. Steinmann, R. Jaramillo, K. Hartman, R. Chakraborty, P. Sinsermsuksakul, D. Chua, T. Buonassisi, and R. G. Gordon, Co-optimization of SnS absorber and Zn(O,S) buffer materials for improved solar cells, Prog. Photovoltaics Res. Appl. **23**, 901 (2015).

[25] H. Noguchi, A. Setiyadi, H. Tanamura, T. Nagatomo, and O. Omoto, Characterization of vacuum-evaporated tin sulfide film for solar cell materials, Sol. Energy Mater. Sol. Cells **35**, 325 (1994).

[26] A. Sánchez-Juárez, A. Tiburcio-Silver, and A. Ortiz, Fabrication of SnS_2/SnS heterojunction thin film diodes by plasma-enhanced chemical vapor deposition, Thin Solid Films **480-481**, 452 (2005).

[27] J. Y. W. Seto, The electrical properties of polycrystalline silicon films, J. Appl. Phys. **46**, 5247 (1975).

[28] F.-Y. Ran, Z. Xiao, H. Hiramatsu, H. Hosono, and T. Kamiya, Growth of high-quality SnS epitaxial films by H_2S flow pulsed laser deposition, Appl. Phys. Lett. **104**, 072106 (2014).

[29] B. Zhou, S. Li, W. Li, J. Li, X. Zhang, S. Lin, Z. Chen, and Y. Pei, Thermoelectric properties of SnS with Na-doping, ACS Appl. Mater. Interfaces **9**, 34033 (2017).

[30] S. S. Hegde, A. G. Kunjomana, P. Murahari, B. K. Prasad, and K. Ramesh, Vacuum annealed tin sulfide (SnS) thin films for solar cell applications, Surf. Interfaces **10**, 78 (2018).

[31] Y. Kawano, J. Chantana, and T. Minemoto, Impact of growth temperature on the properties of SnS film prepared by thermal evaporation and its photovoltaic performance, Curr. Appl Phys. **15**, 897 (2015).

[32] *Handbook of Transparent Conductors*, edited by D. S. Ginley (Springer US, Boston, 2011).

[33] K. T. Ramakrishna Reddy, N. Koteswara Reddy, and R. W. Miles, Photovoltaic properties of SnS based solar cells, Sol. Energy Mater. Sol. Cells **90**, 3041 (2006).

[34] A. Schneikart, H.-J. Schimper, A. Klein, and W. Jaegermann, Efficiency limitations of thermally evaporated thin-film SnS solar cells, J. Phys. D Appl. Phys. **46**, 305109 (2013).

[35] M. Sugiyama, K. T. R. Reddy, N. Revathi, Y. Shimamoto, and Y. Murata, Band offset of SnS solar cell structure measured by x-ray photoelectron spectroscopy, Thin Solid Films **519**, 7429 (2011).

[36] P. Sinsermsuksakul, K. Hartman, S. Bok Kim, J. Heo, L. Sun, H. Hejin Park, R. Chakraborty, T. Buonassisi, and R. G. Gordon, Enhancing the efficiency of SnS solar cells via band-offset engineering with a zinc oxysulfide buffer layer, Appl. Phys. Lett. **102**, 053901 (2013).

[37] P. Sinsermsuksakul, L. Sun, S. W. Lee, H. H. Park, S. B. Kim, C. Yang, and R. G. Gordon, Overcoming efficiency limitations of SnS-based solar cells, Adv. Energy Mater. **4**, 1400496 (2014).

[38] L. Sun, R. Haight, P. Sinsermsuksakul, S. Bok Kim, H. H. Park, and R. G. Gordon, Band alignment of SnS/Zn(O,S) heterojunctions in SnS thin film solar cells, Appl. Phys. Lett. **103**, 181904 (2013).

[39] H. Yun, B. Park, Y. C. Choi, J. Im, T. J. Shin, and S. Il Seok, Efficient nanostructured TiO_2/SnS heterojunction solar cells, Adv. Energy Mater. **9**, 1901343 (2019).

[40] S. Lin, X. Li, H. Pan, H. Chen, X. Li, Y. Li, and J. Zhou, Numerical analysis of SnS homojunction solar cell, Superlattices Microstruct. **91**, 375 (2016).

[41] S. Kawanishi, I. Suzuki, S. R. Bauers, A. Zakutayev, H. Shibata, H. Yanagi, and T. Omata, SnS homojunction solar cell with *n*-type single crystal and *p*-type thin film, Sol. RRL **5**, 2000708 (2021).

[42] B. Ghosh, R. Bhattacharjee, P. Banerjee, and S. Das, Structural and optoelectronic properties of vacuum evaporated SnS thin films annealed in argon ambient, Appl. Surf. Sci. **257**, 3670 (2011).

[43] W. Huang, S. Cheng, and H. Zhou, Electrical and optical properties of In-doped SnS thin films prepared by thermal evaporation, ECS Trans. **44**, 1295 (2012).

[44] Y. Liu, K. Cao, J. Liu, Z. Zhang, J. Ji, F. Wang, and Z. Li, Electrodeposition of copper-doped SnS thin films and their electric transmission properties control for thermoelectric enhancement, J. Mater. Sci. Mater. Electron. **30**, 15880 (2019).

[45] V. R. Minnam Reddy, S. Gedi, C. Park, M. R. W., and R. R. Ramakrishna, Development of sulphurized SnS thin film solar cells, Curr. Appl. Phys. **15**, 588 (2015).

[46] B. Jang, S. Yeo, H. Kim, B. Shin, and S.-H. Kim, Fabrication of single-phase SnS film by H_2 annealing of amorphous SnS_x prepared by atomic layer deposition, J. Vac. Sci. Technol. A: Vac. Surf. Films **35**, 031506 (2017).

[47] L. Zhao, Y. Di, C. Yan, F. Liu, Z. Cheng, L. Jiang, X. Hao, Y. Lai, and J. Li, In *situ* growth of SnS absorbing layer by reactive sputtering for thin film solar cells, RSC Adv. **6**, 4108 (2016).

[48] E. A. Kraut, R. W. Grant, J. R. Waldrop, and S. P. Kowalczyk, Precise Determination of the Valence-Band Edge in X-Ray Photoemission Spectra: Application to Measurement of Semiconductor Interface Potentials, Phys. Rev. Lett. **44**, 1620 (1980).